

A DESIGN METHOD FOR INVESTIGATING CAVITATION DELAY

Wesley H. Brewer, James C. Newman, III, Greg W. Burgreen, Clarence O. E. Burg
Computational Simulation and Design Center,
Mississippi State University
wbrewer@erc.msstate.edu

ABSTRACT

A method is proposed as a means to systematically investigate cavitation delay. The proposed method uses an unstructured RANS solver, with the ability to compute sensitivity derivatives via a Complex Taylor series expansion (CTSE) method. The localized region affecting cavitation inception is parameterized and represented by a minimal amount of control points, using either Non-Uniform Rational B-Splines or a Bezier patch/curve. An objective function is formulated to maximize the minimum pressure in the trailing vortex system. This method is used to develop and evaluate conceptual shapes for cavitation alleviation. Sensitivity derivatives are used to assess the dependence of the localized region on the minimum pressure region, and to drive the localized modification to the optimal shape for cavitation delay.

Using this method, conceptual shapes of cavitation alleviation are generated and demonstrated on three example applications: (1) a structured simulation/optimization of an open-water propeller, (2) an unstructured simulation/optimization of a ducted propulsor, and (3) an unstructured CFD-based design of the diffuser of a rotary blood pump. In the case of the open-water propeller, the minimum and average pressure on the blade tip is increased by 5% and 22% respectively. In the case of the ducted propulsor, where tip-leakage vortex cavitation was prevalent, it was shown that modifying the duct geometry can, in fact, completely de-couple the vortex interaction, while simultaneously increasing the pressure in the leakage vortex core region. The rotary blood pump is shown to significantly reduce rotational flow while suppressing a ring-vortex formation and shedding in the diffuser.

NOMENCLATURE

a	average radius of vortex core
β_i	design variable
\tilde{B}	Bernstein polynomials
F	objective function
h	step size for numerical differentiation
i	index of design variable
n	number of design variables
P	non-dimensional pressure, = $pressure / \frac{1}{2}U^2$
U	freestream velocity
t_x, t_r	parametric definition of x and r respectively
y', z'	perturbed geometry locations

INTRODUCTION

Cavitation has plagued pump and propulsors designers for decades. Not until recently has computational fluid dynamics been proven a valid means of even predicting cavitation inception (e.g. see (Farrell, 2000)) much less designing its mitigation. The notion of "improving cavitation performance" greatly depends on the design interests. In this context, we are primarily concerned with delaying the inception (or onset) of cavitation. For submarines, delaying cavitation inception results in the ability to maintain acoustic-stealth behavior at higher speeds and shallower distances. For surface ships, delaying cavitation inception may help to reduce damaging vibratory forces, or improve propulsor efficiency. In the case of cruise liners, improving cavitation performance may reduce the pressure pulsations felt on the aft hull, and thus improve passenger acoustics and satisfaction. For pump designers, improving cavitation performance may provide pumps with much longer life-

cycles.

Much progress has been made over the years in developing advanced propulsion systems to delay cavitation. In general, cavitation can be categorized into three primary manifestations: sheet, cloud, and vortex. Sheet cavitation, also would be called attached cavitation, can typically be thought of as a separation bubble caused by a local minimum pressure. This sheet cavity can be very stable, or highly unstable. The nature of sheet cavitation and inception is understood relatively well (e.g. see (Brewer and Kinnas, 1997)).

For the most part, in the case of open-water propellers, inception occurs in the tip-vortex. Moreover, for the case of ducted propulsion, cavitation inception appears to be a result of a complex interaction between the trailing edge and leakage vortex (Brewer, 2002). With any manifestation of cavitation, the objective is the primarily the same: to increase the localized minimum pressure. Of course, locally increasing the minimum pressure may induce cavitation to occur in another manifestation that was previously not a problem. Hence, the problem of delaying cavitation, especially vortex cavitation, is not trivial.

One of the most formidable problems in cavitation inception prediction has been that of ducted propulsion. The great complexity of these flows as well as advanced geometry shapes drive the need for numerical codes which can handle both the increasing complexity of the geometries as well as the increasing complexity of the flowfields. In this work, these problems are addressed with unstructured Reynolds-Average Navier-Stokes (RANS) solver, which is also capable of computing sensitivity derivatives. Sensitivity analysis allows for the ability to also compute gradient-based information, which will give valuable information on how geometry modifications affect cavitation inception.

The unstructured approach can handle arbitrarily complex geometries, via a completely automated gridding approach. Furthermore, it is desirable that local geometry regions be controlled by a minimal amount of control points. This process of representing the actual geometry by control points is called parameterization.

It must be stated here that computational design optimization in no way is suggested to replace present design methodologies. The intent of design optimization is not to do preliminary or primary design, but to be used to supplement the design process, by making improvements on initial designs in areas where no design methodologies exist. For example, it can be used to reshape propeller tips to delay cavitation. Or it can be used to investigate inlet waterjet profile shapes. It can be used for integrated propulsor hull design optimization. Figure 1 shows a realistic view of

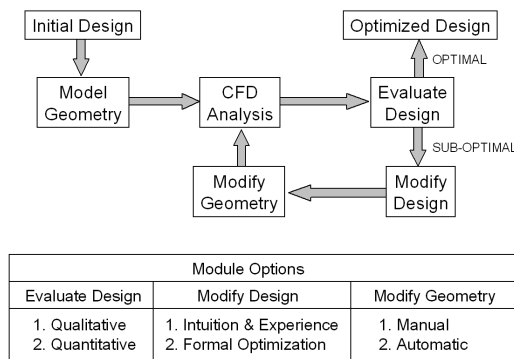


Figure 1. Flow chart of a CFD-based design process.

the design process (Burgreen et al., 2001). The overall goal of the design optimization process is to systematically evolve from some initial design to an optimized design. The main modules of the design process include: (1) CFD analysis, (2) design evaluation, (3) design modification, and (4) geometry modification. The choice of module options allows a design strategy to be defined as simple or complex as one desires. In practice, we have found that all of the options may be exercised in various combinations during the design cycle. Early in the design cycle, the human intellect proves to be the best “optimizer” in conjunction with a “cut-and-try” approach (i.e., option 1 for all modules). When starting from a fairly good design, formal optimization (i.e., option 2 for all modules) is most effective to locate non-intuitive designs.

The main components of CFD-based design optimization, with suggestions for what techniques represent the current state-of-the-art in computational design optimization methods:

1. *Grid generation*: uses unstructured grid capability for arbitrary shape deformation with automated grid re-meshing capabilities.
2. *Parameterization*: uses Non-uniform Rational B-Splines (NURBS) to represent the geometry in 3D, and B-Splines or Bezier curves in 2D/axisymmetric cases.
3. *Flow solver*: uses finite-volume with Roe’s flux formulation, with ability for Detached Eddy Simulation in areas of interest
4. *Gradient computation*: Ability to compute first and second derivatives using sensitivity derivative approach via Complex Taylor Series Expansion method.
5. *Objective function*: uses predictive bubble dynamics model for accurate prediction of cavitation inception.

Each of these components is exemplified using three test cases: (1) an open-water propeller (P5168), (2) a ducted propulsor (P5206), and (3) the diffuser of

a rotary blood pump. Each of these aspects will be discussed in detail, and examples will be drawn from each of the three cases.

BACKGROUND

Many ideas have been studied for the reduction of cavitation inception. There is an abundance of literature on tip vortex cavitation, pump cavitation, tip-leakage vortex computation, and optimal propulsor design. The major works related to optimal tip and duct design in relation to cavitation are presented here.

Optimal propeller tips

Platzer and Souders give a comprehensive listing of designs to alleviate tip-vortex cavitation in (Platzer and Souders, 1979). Platzer and Souders present seventeen different designs for tip vortex alleviation and cite relevant research that support each design. These concepts include mass injection, end plates, delta tips, porous tips, splines, honeycomb, contra-vanes, tip bulbs, serrated edges, ogee tips, drooped wings, and winglets. Later, Souders and Platzer (Souders and Platzer, 1981) experimentally studied various tip bulb designs. They also investigated the effect of roughness on cavitation inception, as well as mass injection. They noted 94% increase in inception speed for the roughened tip, 38% percent for the bulbous tip, 54% for the active mass-injected tip, and 33% for the passive mass-injected tip. These gains were made with negligible loss in performance.

Among these designs, two stand out as promising: the tip bulb and mass injection (Jessup, 2000). Platzer noted that the bulb must be carefully designed both to minimize cavitation inception and to maintain efficiency. Crump (Crump, 1948) also experimentally studied the tip bulb design. He noted 25% improvements in cavitation inception speed.

Since Platzer and Souders, several new propeller tip concepts have been demonstrated: notably, “the ducted tip” by Green (Green and Duan, 1995) and the “tip-fin” by Anderson (Anderson, 1998). Kuiper (Kuiper, 2001) studied optimal inception speed by experimentally investigating the effects of skewness on cavitation inception.

Optimal duct casing

Related to ducted propulsors, Farrell (Farrell, 1987) discussed the effects of “trenching,” which consists of the tip riding in a groove or trench in the duct. He also discussed several effective tips in ducted rotor design: the flat tip, the grooved tip, the squealer tip, winglets, and the knife tip. Experimental data is presented from Shuba (Shuba, 1983) in which he plots

cavitation number as a function of dimensionless tip clearance, λ . The data shows an optimal tip clearance (lowest cavitation inception number) of about $\lambda \approx 0.2$. Farrell also reviewed duct casing treatment methods, such as: circumferential grooves, axial-skewed slots, and blade angle slots.

Jia et al. (Jia et al., 2001) numerically investigated three different tip gap shapes and its effects on the leakage vortex. They studied the following three configurations: zero gap, uniform gap, and linearly varying gap (both expanding and shrinking). The linearly expanding is shown to give the highest efficiency.

Design optimization for marine propulsors

There has been much work recently in the area of design optimization of marine propulsors. Mishima (Mishima, 1996) studied the design of cavitating propeller blades using gradient-based numerical optimization. Black (Black, 1995) developed a method for computing optimum blade sections by using a 2D interactive potential panel method and boundary layer solver in a strip-wise sense. He used genetic algorithms to perform the optimization and included such design constraints as cavitation inception prediction, lift/drag maximization, and flow separation avoidance. Coney (Coney, 1989) developed a method to compute optimum radial circulation distributions for a circumferentially averaged inflow. Traditionally, this is the first step in designing a propeller. One would then use an inverse method to design the blade which would produce the given circulation distribution (Kerwin, 1973, Kerwin et al., 1994).

The previous methods use a potential-based panel methods as an analysis tool. Performing optimization on more complex geometries will require solving the Reynolds-Averaged Navier-Stokes (RANS) equations.

Computational design optimization

Computational design has become an active area of research in the hydrodynamic community. Although simulation has been used in the design of hydrodynamic configurations in the past, only those that utilize sensitivity derivatives and gradient-based optimization methods will be considered in this review. A detailed and concise overview of sensitivity analysis methods and aerodynamic design optimization research may be found in Newman et al. (Newman et al., 1999).

Hino (Hino, 1999) used the Navier-Stokes equations coupled with a sequential quadratic programming (SQP) method to minimize the wave and viscous drag on ship hull forms. In that work, Hino adopted a discrete-adjoint variable approach to compute sensi-

tivity derivatives and redesigned a hypothetical tanker hull and a Series 60 hull for minimum resistance. Subsequently, based on Jameson's (Jameson, 1988) work, Cowles and Martinelli (Cowles and Martinelli, 2000) described a control-theory (continuous) approach to sensitivity analysis for incompressible, turbulent viscous flows and applied this approach to match target pressure distributions (inverse design) on finite span wings and sails. Tahara et al. (Tahara et al., 2000) used a Navier-Stokes code, with finite-difference gradients, for CFD-based design of the bow bulb on a surface combatant. In Tahara no free surface effects were considered, and the objective was to minimize the downstream vorticity in the vicinity of the bulbous bow. Ragab (Ragab, 2001) describes the use of a continuous-adjoint approach in free-surface potential flow and applies the approach to redesign a baseline ship for minimum wave resistance, and to match target pressure distributions. Soto and Löhner (Soto and Löhner, 2001) proposed an incomplete-gradient adjoint formulation based on the continuous approach to sensitivity analysis where only the adjoint on the boundary of the domain is computed. In their approach the derivatives of the cost or objective function were computed using finite-difference. Soto and Löhner, using the incompressible Euler equations, redesigned 3D hydrofoils to maximize the minimum pressure on pressure and suction surfaces, and to redesign the bow bulb on a surface ship for minimum wave drag. Dreyer and Martinelli (Dreyer and Martinelli, 2000) utilize a continuous-adjoint approach for target pressure matching of propulsor configurations using the pseudo-compressible Euler equations in a rotating frame.

GRID GENERATION

The focus of our present and future work is on unstructured grid generation technologies, rather than on structured grids. The unstructured approach allows fully automated grid generation, with automatic grid error detection and refinement. Furthermore, the unstructured approach allows for virtually perfect load-balancing distributions for improved parallel efficiency. The nodes are re-ordered using a Cuthill-McKee algorithm which greatly improves the cache coherency. In fact, because of this cache-coherency optimization, it is possible to achieve super-linear speedup on a parallel cluster.

AFLR3 (Advancing-Front/Local-Reconnection) was used to generate the unstructured grids (Marcum and Weatherill, 1995). The advancing-front technique is used for the initial placement of points. A combined Delaunay/min-max criterion is then used for re-connecting the points to form volume elements. The code can create tetrahedral, pyramid, quadrilateral,

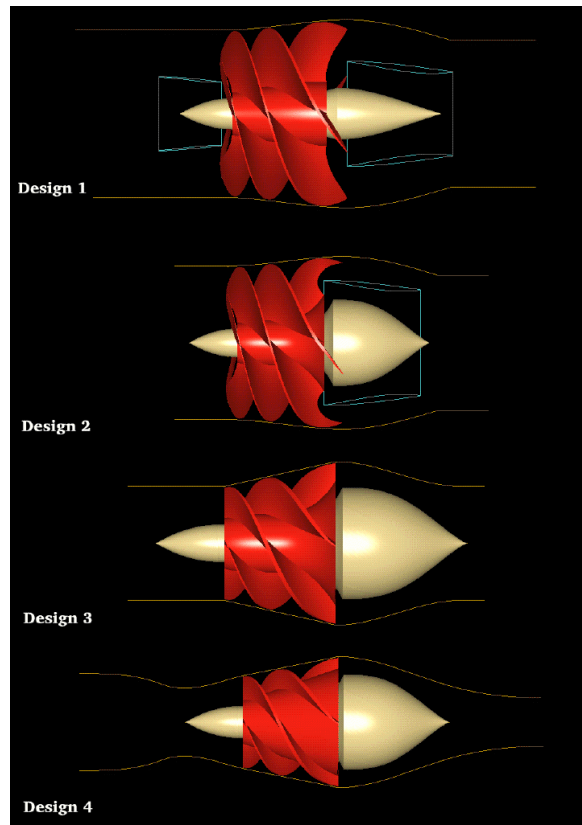


Figure 2. Design evolution of a rotary blood pump (Burgreen and Antaki, 1996).

prismatic, and hexahedral element types.

With regards to computational design optimization, the unstructured mesh can be automatically regenerated within the solution process. This will allow for automated shape modifications in addition to automated grid refinement.

PARAMETERIZING THE GEOMETRY

Parameterization allows the geometry to be represented by a vector of design variables. This is typically done using Bezier or B-Spline representation in 2D or a Bezier patch or NURBS (Non-Uniform Rational B-Spline) surface in 3D.

One could potentially completely parameterize the geometry. This would allow for the maximum number of possible designs. Burgreen (Burgreen and Antaki, 1996) showed that an entire pump can be parameterized using approximately 40 Bezier control points. Since the geometry was primarily axisymmetric, the number of design points was greatly reduced. An example of the different types of shapes generated are shown in Figure 2.

With regards to cavitation delay, we are primarily concerned with parameterizing only a localized region, such that the propulsor performance is not

changed. Practically, we are interested in changing the blade tip shape and/or the duct shape, as to affect the pressure distribution in the trailing vortex. In this case, only small local considerations should be considered, lest the propulsor performance be drastically effected. In this section, we consider two such type of local distortions: (1) modifying the blade tip and (2) modifying the duct surface.

Parameterizing the blade tip

The pressure and suction design surfaces can be parameterized with a Bezier surface which controls the normal thickness variation as:

$$t_n = \sum_{i=0}^N \sum_{j=0}^M P_{ij} \left[\frac{N!u^i(1-u)^{N-i}}{i!(N-i)!} \right] \left[\frac{M!v^j(1-v)^{M-j}}{j!(M-j)!} \right] \quad (1)$$

where P_{ij} are the Bezier control points that were used as the design variables, and u , v represent the parametric variables in the chordwise and spanwise directions, respectively. A two-dimensional example of this parameterization is shown in Figure 3 for an initially symmetric hydrofoil. Geometric constraints were enforced such that slope and curvature would remain unchanged between the pressure and suction surfaces. With these constraints, the total number of design variables reduced to eight. Transfinite interpolation (TFI) of surface deformations into the volume mesh was used to modify the computational mesh to the latest design.

Parameterizing the duct surface.

The degrees of freedom $dim(\beta_i)$ for each control point increases the design space. In other words, for a 3D problem, each control point can represent three design variables. Moreover, each design variable will require performing a separate simulation. Therefore, a single control point with three degrees of freedom will require four separate simulations: (1) no perturbation, (2) perturb in x direction, (3) perturb in y direction, and (4) perturb in z direction.

Therefore, due to the computational cost of computational design optimization, one should judiciously choose a means of representing the problem with a minimal amount of control points. In the case of a ducted propulsor, dimension reduction is used to map three dimensional space into two dimensions, thereby reducing the number of control points from nine to three (for $dim(\beta_i) = 1$). The following table further enumerates the simplification:

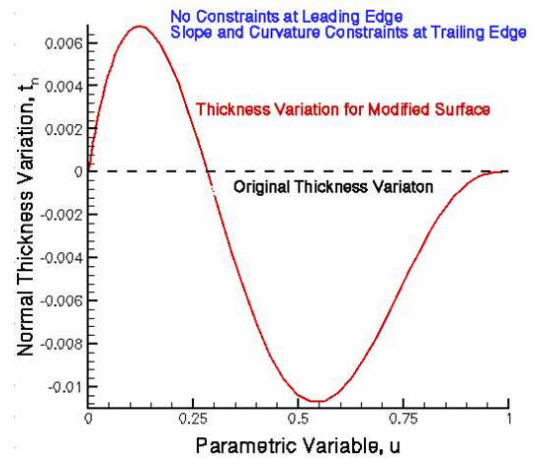
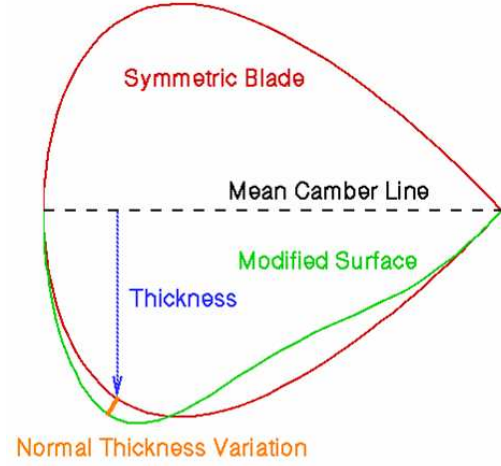


Figure 3. Localized tip parameterization example.

Space	Coordinates	$dim(\beta_i)$: 1	2	3
\mathfrak{R}^3	x, y, z	9	18	27
\mathfrak{R}^2	x, r	3	6	

Figure 4 shows the simplified parameterization for the propulsor unit. All grid points in a specified domain are affected by this parameterization. The affected domain is given as:

$$(x_i, r_i) \in [a, b] \quad (2)$$

where a and b represent the domain lower and upper bounds respectively. The points are moved algebraically according to the following formula:

$$y' = y + f(t_x, \beta_i) \frac{y t_r}{r} \quad z' = z + f(t_x, \beta_i) \frac{z t_r}{r} \quad (3)$$

where t_x and t_r are given by:

$$t_x = \frac{x - x_a}{x_b - x_a} \quad t_r = \frac{r - r_a}{r_b - r_a} \quad (4)$$

and y , z , and r are functions of x , and f is computed by deCasteljau's algorithm. DeCasteljau's algorithm evaluates Bernstein polynomials at t_x . The Bernstein polynomials $\vec{B} = (B_x, B_r)$ are given as:

$$\vec{B}_i^n(t) = \frac{n!}{(n-i)!i!} (1-t_x)^{n-i} t_x^i = \binom{n}{i} (1-t)^{n-i} t^i \quad (5)$$

where $i \in [0, n]$. The Bernstein polynomials are initialized by the control points $\vec{B}_i^0 = \vec{\beta}_i$. The resulting value at a given t_x is:

$$f(t_x, \beta_i) = B_{r0}^n \quad (6)$$

where n here is the number of control points.

It should be noted that this type of parameterization allows two different types of shape modifications depending on r_a and r_b : (1) modify the duct only or (2) modify both the duct and the propeller, keeping the tip gap constant. Thus, the two-dimensional parameterization allows a greater variety of change than a three-dimensional NURBS control net, while requiring much less degrees of freedom.

COMPUTING THE FLOWFIELD

The currently proposed method for computing the flow-field is the Mississippi State University flow solver, **U²NCLE** (**U**nstructured, **U**nsteady **C**omputation of **f**ieLd **E**quations). **U²NCLE** is an unstructured, unsteady Reynolds Averaged Navier-Stokes code. The method uses a finite-volume formulation of the Navier-Stokes equations which takes the conservation laws written in integral form discretized about control volumes. One advantage of this method is that the fluxes can be converted to surface integrals via Green's theorem. Finite-volume schemes are much more suited for solving complicated geometrical problems due to the fact that they can be solved directly in the physical domain. Discretization in the physical space ensures that mass and momentum are conserved also on the discrete level (Hirsch, 1994a).

Governing Equations

To solve the incompressible Navier-Stokes equations using a time marching scheme, an artificial compressibility term is added to the equations following

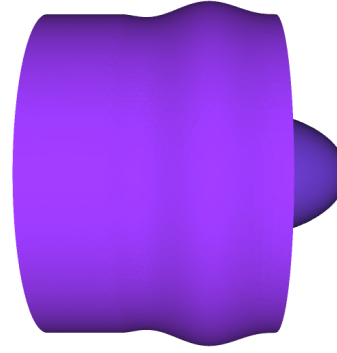
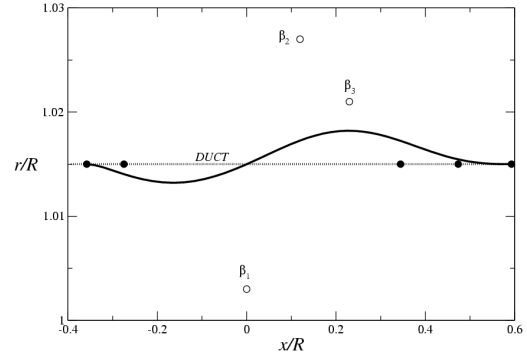


Figure 4. Bezier parameterization of duct. Top: showing control points and slope continuity points. Bottom: showing outer duct geometry.

the method of Chorin (Chorin, 1967). Numerically, this casts the equations into a hyperbolic system with pseudo-pressure waves propagating at a finite speed (Hirsch, 1994b). Additionally, this provides a coupling between pressure and velocity.

The incompressible Navier-Stokes equations are based on the concepts of conservation of mass and momentum, and are given in three dimensions as:

$$\frac{\partial}{\partial t} \int_{\Omega} Q d\mathcal{V} + \int_{\partial\Omega} \vec{F} \cdot \vec{n} dA = \quad (7)$$

$$\frac{1}{Re} \int_{\partial\Omega} \vec{G} \cdot \vec{n} dA + \int_{\Omega} s d\mathcal{V}$$

where

$$Q = \begin{bmatrix} P \\ u \\ v \\ w \end{bmatrix} \quad (8)$$

$$\vec{F} = \begin{bmatrix} \beta u \\ u^2 + P \\ uv \\ uw \end{bmatrix} \hat{i} + \begin{bmatrix} \beta v \\ vu \\ v^2 + P \\ vw \end{bmatrix} \hat{j} + \begin{bmatrix} \beta w \\ wu \\ wv \\ w^2 + P \end{bmatrix} \hat{k} \quad (9)$$

$$\vec{G} = \begin{bmatrix} 0 \\ \tau_{xx} \\ \tau_{yx} \\ \tau_{zx} \end{bmatrix} \hat{i} + \begin{bmatrix} 0 \\ \tau_{xy} \\ \tau_{yy} \\ \tau_{zy} \end{bmatrix} \hat{j} + \begin{bmatrix} 0 \\ \tau_{xz} \\ \tau_{yz} \\ \tau_{zz} \end{bmatrix} \hat{k} \quad (10)$$

$$s = \begin{bmatrix} 0 \\ 0 \\ -\Omega_x w \\ \Omega_x v \end{bmatrix} \quad (11)$$

\vec{G} contains the shear stress components given as:

$$\tau_{ij} = (1 + \mu_t) \left(\frac{\partial u_i}{\partial x_j} + \frac{\partial u_j}{\partial x_i} \right) \quad (12)$$

where i and j are each to be replaced by x, y, z .

The equations are solved in a rotating frame of reference. Thus, a relative velocity is defined such that:

$$\vec{v} = \vec{u} - \vec{\Omega} \times \vec{r} \quad (13)$$

where $\vec{v} = (u_r, v_r, w_r)$ is the velocity and \vec{r} is the position vector, both relative to the rotating frame. Assuming the propeller rotates about the x -axis simplifies the problem, making the rotation vector $\vec{\Omega} = (\Omega_x, 0, 0)$. The resulting absolute velocities are written in terms of the relative components:

$$u = u_r \quad (14)$$

$$v = v_r + \Omega_x z \quad (15)$$

$$w = w_r - \Omega_x y \quad (16)$$

The contributions of the rotating frame reference are handled by the matrix s .

Turbulence Model

U²NCLE has four turbulence models: $k - \epsilon$, $k - \omega$, $q - \omega$, and a one equation Spalart Allmaras¹ model. The turbulence model is solved in an iterative manner with the RANS equations. First, the Navier-Stokes equations are solved to compute the mean flow variables, Q^{n+1} . Then, the turbulence model is solved to compute the turbulent eddy viscosity, μ_t^{n+1} .

Numerics

A median-dual control volume is defined about each node in the domain. Temporal discretization is achieved using a second-order generalized method, which is covered extensively in (Hyams, 2000). The spatial discretization of the inviscid terms is also second order. A ‘‘directional derivative’’ approach is used to discretize the viscous flux vectors, which essentially incorporates solution data at the nodes and edge local data to approximate the tangential and normal derivatives, while the convective flux vectors are linearized using the method of Roe. Barth’s limiter was used to limit the convective terms, while a simple clipping limiter was used to handle the turbulent dependent variables.

The discretized equations must be linearized, where each of the terms not containing Δq^n are moved to the right hand side. This is accomplished by finding q^{n+1} such that:

$$\mathfrak{S}(q^{n+1}) = \frac{\Delta q_i^n}{\Delta t} + \mathfrak{R}(q^{n+1}) = 0 \quad (17)$$

Newton’s method is used to solve this equation as follows:

$$\begin{aligned} \mathfrak{S}'(q^{n+1,m})(q^{n+1,m+1}) &= \\ \mathfrak{S}'(q^{n+1,m})\Delta q^{n+1,m} &= -\mathfrak{S}(q^{n+1,m}) \end{aligned} \quad (18)$$

A symmetric Gauss-Seidel solution algorithm is used to solve the system of discretized equations.

The solver is partitioned into a minimum of 24 blocks, and solved on a parallel IBM super-cluster. Typical run-time for a converged solution is 24 hours.

COMPUTING THE GRADIENTS

Sensitivity derivatives provide information about the sensitivity of the flow to changes in design parameters. Traditionally, modifications are performed on

¹As suggested by (Spalart and Allmaras, 1992), this model was modified to limit the production term to improve numerical dissipation in the vortex region. The implementation is documented in (Hyams, 2000).

a trial and error basis based on intuition. That is to say, if cavitation is occurring, one might say “let’s try rounding the tip a little more”. Sensitivity derivatives will help guide the designer to exactly where the rounding needs to be done.

Differentiation of the partial differential equations can be performed at one of two levels, termed the *continuous* or *discrete* approach. For the continuous (a.k.a. variational) approach, the PDE’s are discretized prior to discretization. The discretization is performed either by hand, or by using Lagrange multipliers. For the discrete approach, the PDE’s are differentiated after discretization. In this work, the discrete approach to sensitivity analysis is used.

With gradient-based optimization methods, the search direction is determined using the first derivatives of the objective and constraint functions with respect to the vector of independent design variables (i.e., sensitivity derivatives). This is not to say that the search direction is solely based on first-derivative information; it is possible to estimate higher-order derivatives using the computed first derivatives. In general, the objective and constraint functions may be expressed as $F_i(Q, X, \beta_k)$. Here, Q represents the disciplinary state vector which is produced from solving the RANS equations, X is the computational mesh, and β_k the vector of design variables. The sensitivity derivatives of these functions may be obtained by direct differentiation with respect to implicit and explicit dependencies as

$$\nabla F_i = \frac{\partial F_i}{\partial \beta_k} + \left(\frac{\partial F_i}{\partial Q} \right) \frac{\partial Q}{\partial \beta_k} + \left(\frac{\partial F_i}{\partial X} \right) \frac{\partial X}{\partial \beta_k} \quad (19)$$

Numerical Differentiation

Numerical differentiation is used to compute the state vector, $\partial Q / \partial \beta_k$, and the grid sensitivity terms, $\partial X / \partial \beta_k$. These derivatives can either be computed by a finite-difference approach, or by the Complex Taylor Series Expansion (CTSE) method (developed by Newman et al. (Newman et al., 1998)).

For a central finite-difference approximation to the derivative, one may expand the function in a Taylor series about a given point using a forward and a backward step, and then subtracting to yield

$$\frac{df}{dx} = \frac{[f(x+h) - f(x-h)]}{2h} - \frac{h^2}{3!} \frac{d^3f}{dx^3} - \frac{h^4}{5!} \frac{d^5f}{dx^5} - \dots \quad (20)$$

This expression for the derivative has a truncation error of $O(h^2)$. The advantage of a finite-difference approximation to obtain sensitivity derivatives is that any existing code may be used without modification.

The disadvantages of this method are the computational time required and the possible inaccuracy of the derivatives.

The CTSE method uses complex variables to approximate derivatives of real functions. Instead of the finite-difference approximation, consider expanding the function in a Taylor series using a complex step as

$$f(x+h\hat{i}) = f(x) + h\hat{i} \frac{df}{dx} - \frac{h^2}{2!} \frac{d^2f}{dx^2} - \frac{h^3\hat{i}}{3!} \frac{d^3f}{dx^3} + \dots \quad (21)$$

where $i = \sqrt{-1}$. Solving this expression for the imaginary part of the function yields

$$\frac{df}{dx} = \frac{Im[f(x+h\hat{i})]}{h} + \frac{h^2}{3!} \frac{d^3f}{dx^3} - \frac{h^4}{5!} \frac{d^5f}{dx^5} + \dots \quad (22)$$

This expression for the derivative also has a truncation error of $O(h^2)$. By evaluating the function with a complex argument, both the function and its derivative are obtained, without subtractive terms, and thus cancellation errors are avoided. The real part is the function value to second order.

Figure 5 shows an error analysis of a sample function derivative approximated using forward difference, central difference, and the CTSE method. In this figure, the error between the exact derivative and the approximation drops at the same rate for the central difference and CTSE methods, demonstrating that they converge at the same rate. The error for the forward difference approximation reduces at a difference rate, showing that it converges only linearly. At some point, the round-off error for the forward difference and central difference methods is approximately the same as the error from the nonlinearity of the function. As the step size h decreases beyond this optimal point, the error in the finite difference approximations grows until the finite difference approximation to the derivative is 0 and the error is value of the derivative. However, for the CTSE method, the error continues to decrease at a constant rate until the error reaches machine zero. Once the step size is small enough so that the error is machine zero, then the derivative value is constant. Since the derivative approximated by the CTSE method is accurate machine precision over a wide range of step sizes, this method is a “step size” independent method. Therefore, the choice of the step size, which is a serious problem for the finite difference methods, is trivial.

The CTSE method has several advantages over the finite-difference approach:

1. Method is equivalent to a discrete-direct approach (see (Burg and Newman, 2003))

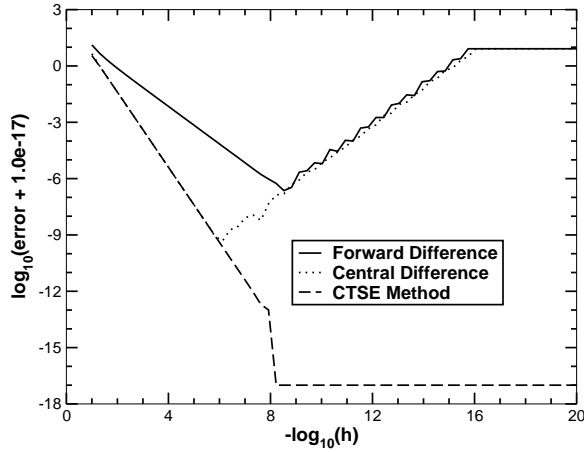


Figure 5. Effect of step size h on derivative error, comparing forward and central difference methods and the CTSE method.

2. Unlike the finite-difference approximation, fully converged flow solutions are not required to obtain derivatives of sufficient accuracy for design.
3. The method is not sensitive to step size selection and only requires step sizes that avoid excessive truncation error; thus, it has been shown that this method demonstrates true second-order accuracy
4. The CTSE technique can be used to compute second derivative information using available data, but these computations are subject to cancellation errors.

Updating the Design Variables

With the method of steepest descent, the design variables are updated utilizing only the first derivative in conjunction with Newton's method as follows:

$$\Delta\beta_i = -\alpha\nabla F \quad (23)$$

where ∇F is the optimal search direction and α is the step size in that direction. In general, we use $\alpha = \frac{F}{\|\nabla F\|^2 + \epsilon}$ where $\epsilon \approx 10^{-8}$ is used to prevent division by zero.

FORMULATING AN OBJECTIVE FUNCTION

An objective function accurately quantifies the success of the design modification. Ideally, the objective function should be evaluated from within the RANS solution process. However, it can also be evaluated as a post-processing option, in which case the user runs the design iterations manually: first running the flow solution, then manually computing the objective function, manually computing the sensitivity derivatives, manually modifying the geometry, and then re-running the flow solution.

To delay cavitation inception, the obvious objective would be to increase the pressure in regions where inception is known to occur. The following objective function can be used to do this:

$$F = \sum_{i=0}^{i=N} (P_i - P_{avg})^2 e^{-\left(\frac{P_{avg}}{P_{target}}\right)} \quad (24)$$

where P_{target} is the target pressure (the desired pressure to reach at the minimum pressure location), P_{avg} is the average pressure over a given region of points, and N is the number of vertices in the domain. This function tends to drive the pressure to the target by increasingly weighting those points below and above the target. It is important to increase the average pressure over a localized region, so that a continuous solution can be achieved.

For the case of sheet cavitation, locating the region of minimum pressure is rather trivial (e.g. see (Brewer and Kinnas, 1997)). However, for the case of vortex inception, the task is much more challenging, and involves accurately computing and tracking the trailing vortex structure.

Vortex analysis method

In the case of tip vortex inception, we would simply want to locally increase the minimum pressure in the vortex core. Practically, it is difficult to implement this type of requirement because the minimum pressure location is highly grid dependent and tends to move based on slight changes in geometry and inflow conditions. Therefore, it becomes labor-intensive process to track the minimum pressure. The author has developed a means of automatically tracking the minimum vortex pressure via a vortex analysis method (Brewer, 2002). Given the vortex centers and various locations along the core, the vortex analysis method can be used to compute pressure, vorticity, and circulation along the core. Figure 6 shows the vortex analysis method on the P5206 ducted propulsor. Currently, this is done at the post-processing level. However, ideally this should be performed within the solution process.

Bubble dynamics

In the case of tip-vortex cavitation, one would ideally want to use a Lagrangian bubble dynamics solver to predict when cavitation will occur. However, this may be a laborious process and may be very costly in the case when many design iterations must be conducted. Therefore, practically we attempt to raise the minimum pressure in localized regions where cavitation was known to be a problem.

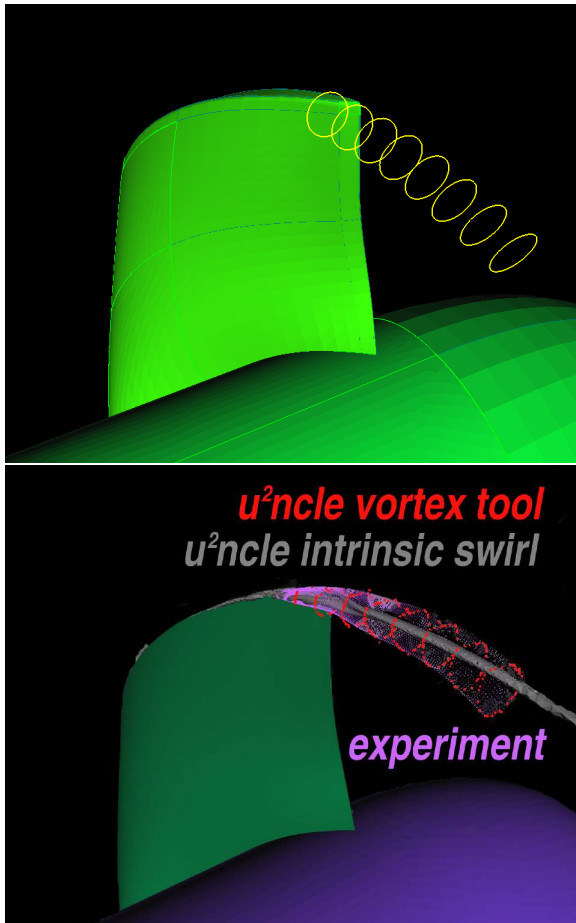


Figure 6. Vortex analysis method is used to compute the minimum pressure, tangential velocities, and diameter along the vortex core. Above: showing line integration paths use to compute vortex circulation. Below: method is validated with experimental results.

Before one can begin to improve cavitation inception performance, one must be able to accurately compute the inception physics. The most ideal and physically correct way to formulate the objective function in this case would be to use a combined RANS simulation and Lagrangian bubble dynamics solver (e.g. see (Farrell, 2000)). The Lagrangian bubble dynamics solver would be able to predict inception by calculating the event rate of bubble explosions. Currently, this methodology is not implemented in Mississippi State's unstructured flow solver.

Vortex/surface correlation

Due to the complexity of tracking the minimum pressure in the vortex core, a simplification can be made: *it can reasonably be assumed that the minimum pressure in the vortex core closely follows the minimum pressure on the blade tip.* Therefore, the objective becomes to maximize the minimum pressure on a specific region of the blade tip surface, rather than

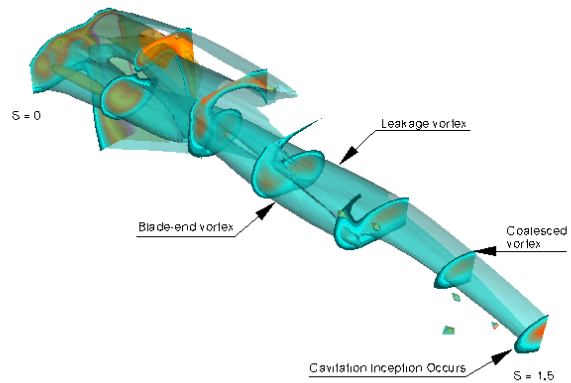


Figure 7. Streamwise velocity isosurface of vortex interaction

the minimum pressure in the vortex core. Equation 24 can be used to evaluate this function value.

Inception on a ducted propulsor

Not until recently has inception on a ducted rotor been well understood. Recent experiments by Chesnakas and Jessup (Chesnakas and Jessup, 2003) and corresponding simulations by Brewer (Brewer et al., 2003) revealed that inception on a ducted rotor is induced by a complex vortex interaction between the trailing edge and leakage vortex. Figure 7 shows an overview of this vortex interaction. Inception occurs a half of a chord length downstream. The trailing edge vortex is stretched around the leakage vortex causing the vortex to be stretched. The vortex stretching results in a reduction of vortex diameter, thus resulting in a faster core spin. Although the RANS simulation cannot accurately all of these details, this understanding provides some guidance to how to formulate the objective function. Therefore, due to the complexity of the problem, the objective here can be to do one or all of the following:

1. completely decouple the two interacting vortices
2. increase the pressure in the vortex core
3. increase the pressure felt on the duct by the leakage vortex

These concepts are evaluated on the P5206 ducted propulsor and will be discussed in the next section.

APPLICATION EXAMPLES

Three applications are used to demonstrate the methods of computational design optimization: (1) an open-water propeller, (2) a ducted propulsor, and (3) the diffuser of a rotary blood pump. Each case uses different approaches to accomplish the task of design

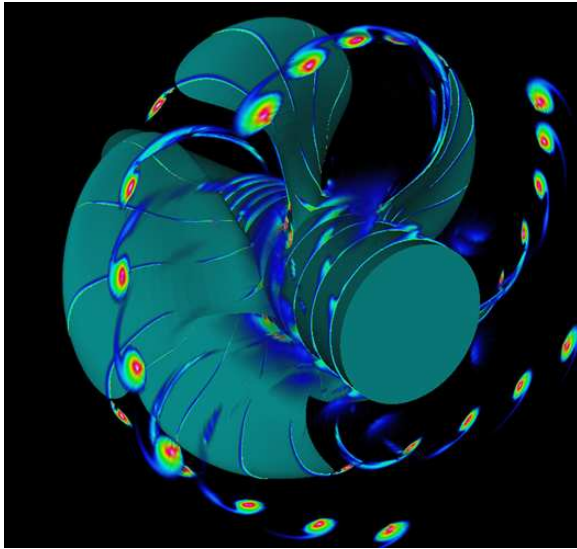


Figure 8. P5168 Geometry and tip vortices.

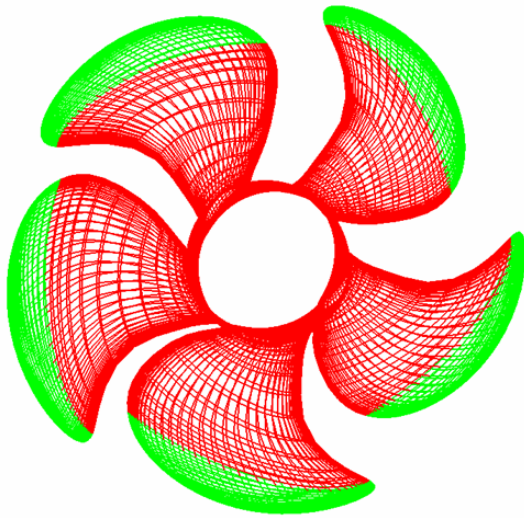


Figure 9. P5168 mesh showing design surface.

improvement. However, each case is successful in producing geometries which improve the flowfield.

Case 1: Open-water propeller

For the open-water propeller study, propeller 5168 (P5168) was selected. P5168 is a five bladed controllable pitch propeller, and was tested in Carderock Division, Naval Surface Warfare Center's 36-inch water tunnel. This propeller was used by ONR for validation purposes of CFD codes in predicting tip vortex flows about Navy surface ship propellers. The ultimate goal of ONR was to demonstrate the usefulness of CFD codes in ranking various candidate blade tip geometries to suppress tip vortex cavitation. The geometry and tip vortices, as predicted via UNCLE, are shown in Figure 8.

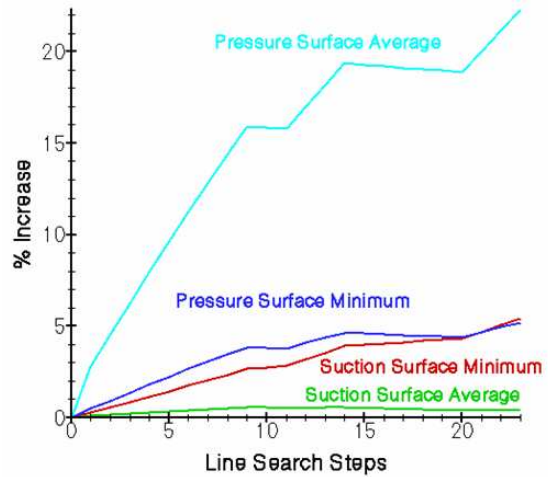


Figure 10. Optimization results for P5168 redesign.

The analysis used the incompressible version of UNCLE and the viscous simulation was performed in parallel with ten blocks. The flow Reynolds number was 4.26×10^6 with an advance ratio of 1.1. Sensitivity derivatives were obtained via the direct approach with the Complex Taylor Series Expansion method used to construct all linearizations.

Since this was an exploratory study, only slight design improvement over the original P5168 propeller was sought. To this end, only one design cycle was performed with 23 line-search steps taken (i.e., only one search direction was computed and transversed). The results of this design cycle are shown in Figure 10. As seen, the minimum and average pressure on the suction design surface has been increased by 5.4% and 0.4%, respectively, and the minimum and average pressure on the pressure design surface has been increased by 5.2% and 22.3%, respectively. The blade shape for this design cycle became more bulbous on the pressure side while introducing a cusp near the trailing edge on the suction side. The normal thickness variation for the pressure and suction surfaces are shown in Figure 3. The pressure on the suction surface and the change in pressure between optimized and original are depicted in Figure 10. As seen, the lowest surface pressure occurs at the trailing edge tip and, thus, this is the region of greatest increase.

It should be noted that if additional design cycles were performed, the shape of the propeller would be expected to continue to evolve until the optimum is attained. However, if the shape is progressing towards a design that exhibits undesirable features, or manufacturability difficulties, the optimization problem can be reformulated with additional constraints and/or objective functions. Thus, the propeller shape after this first design cycle may or may not be indicative of the final design.

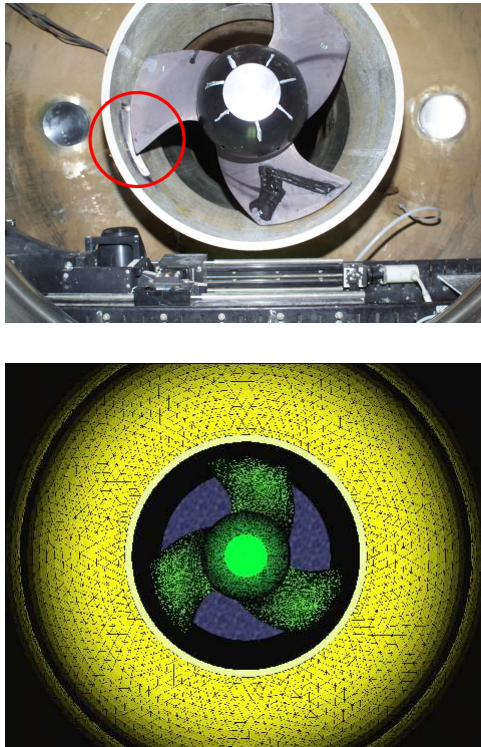


Figure 11. Model and grid of propeller face. Top: Actual P5206 Propeller in 36-in water tunnel (circle denotes window cutout for LDV/PIV measurements). Bottom: Unstructured grid of P5206.

Case 2: ducted propulsor

A three-bladed ducted rotor, which is typical of a ducted submarine propulsor was used to study cavitation inception. Judge et al. (Judge et al., 2001) provides details of the experiment.

Figure 11 shows a photograph of the 34-inch diameter ducted rotor, mounted in the 36-inch water tunnel. The propulsor geometry is given in detail in (Brewer, 2002). The blade has a constant chord length in the radial direction of $c/D = 0.446$. The hub and shaft was modeled as a constant diameter ($D = 13.847$ inches) and extended upstream to the inflow boundary. The fairwater geometry is given in (Brewer, 2002).

Our design optimization process was applied to the P5206 propulsor in attempts to improve cavitation performance. However, the gradients were not able to be implemented because a sufficient level of convergence could not be reached (most likely due to using a limiter in the flow solver). In other words, the “converged” global residual from the flow solver must be much lower than the step size used for differentiation h (refer to Figure 5).

Therefore, instead of computing the gradients, a parametric study was performed by systematically adjusting the control points. For example, one control point was evaluated at three different locations, and

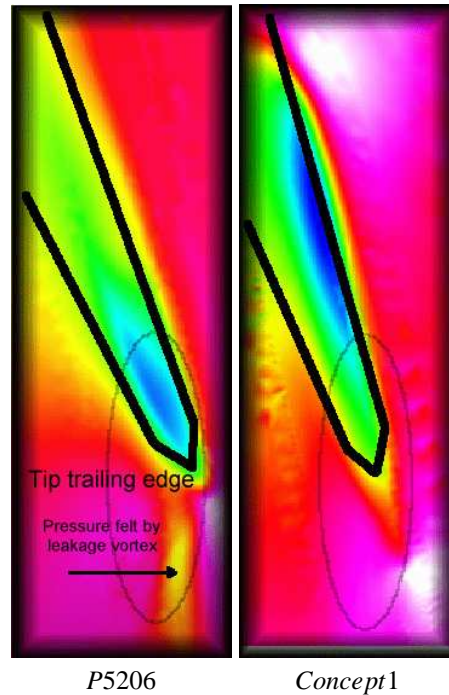


Figure 12. Pressure comparison on duct for original design and concept1. The minimum pressure is moved closer to the leading edge of the blade, and the pressure in the vortex region is significantly increased.

the function value was evaluated for each case. In doing this in a systematic manner, a local minimum can be found.

From this investigation, two amazing results were found. First, the pressure in the trailing vortex region was substantially increased, as shown in Figure 12. Secondly, the leakage and tip vortices became completely decoupled as shown in Figure 14.

To assess the validity of these conceptual designs, they should be studied both numerically, via a Lagrangian bubble dynamics analysis, and experimentally.

Case 3: rotary blood pump

The outlet diffuser of a rotary blood pump was designed using the concepts presented herein (Burgreen and Antaki, 1996, Burgreen and Antaki, 1998, Burgreen and Baysal, 1996, Burgreen et al., 2001). Although cavitation was not the primary design consideration in this case, the functional objectives are still very similar. Rather than suppressing cavitation, the focus instead is placed on biological performance criteria specifically related to blood damage. The most crucial performance criteria in blood pump design are indices of blood damage derived from deleterious fluid dynamic disturbances, direct forces, and/or time exposures to non-biocompatible

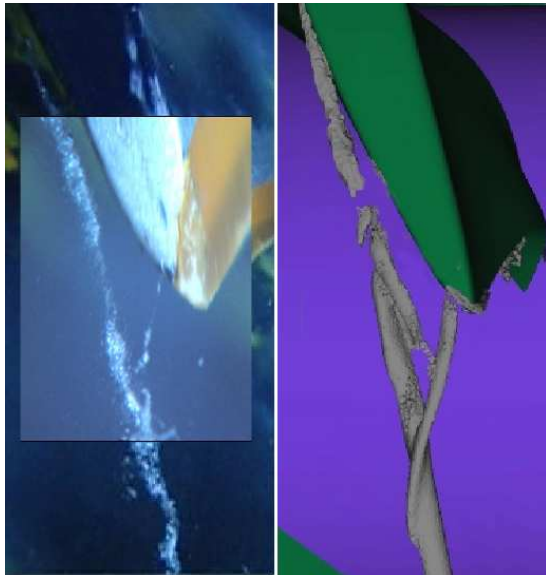


Figure 13. Cavitation comparisons with experiment. Left: the P5206 showing cavitating leakage-vortex. Right: simulation showing constant iso-surface of intrinsic swirl parameter

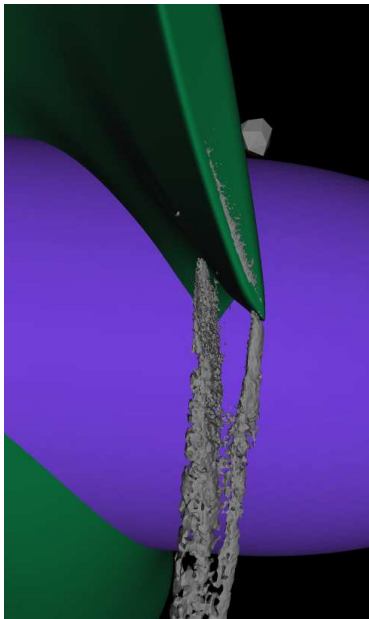


Figure 14. The re-designed propulsor showing the two vortices completely decoupled.

surfaces. In other words, the blood pump designer must optimally combine hematologic design with hydraulic design. This requires that Virchow's triad of coagulation (i.e., the synergistic interaction between blood, surface, and flow) be integrally combined with traditional pump design methods.

For this application, the goal was to reduce thrombogenesis by increasing surface washing, while simultaneously maintaining good pressure recovery (for hydraulic performance) in the diffuser. To accom-

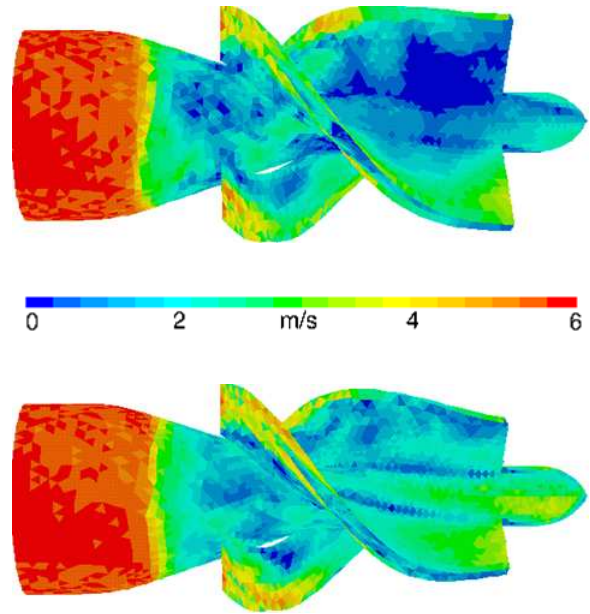


Figure 15. Contours of near-surface velocity magnitude (m/s) for the initial design (top) and the optimal design (bottom) outlet stators.

plish this, the optimization problem was formulated as an objective function-flow constraint combination. The static pressure rise through the diffuser was constrained to be greater or equal to its initial value. The objective function was defined as: maximize the average near-surface velocity magnitude.

The near-surface velocity magnitudes for the initial and optimized designs are shown in Figure 15. The optimal design demonstrates significant reductions of stagnant flow. In the initial design, a small region of flow separation at the rotor hub occurs immediately upstream of the stator blade inlet. This separated region will be shown to significantly influence the fluid dynamics of the stator. In the optimal design, practically no flow separation occurs upstream of the stator blade, and the degree of flow stasis interior to the blades is greatly reduced. Low flow regions at the suction side blade tips evidence flow separation occurring adjacent to the outer housing at the stator blade exit. Excellent agreement is observed between computational results and experimental measurements.

Figure 16 shows the initial and optimized housing shapes for the outlet diffuser. The housing forms a single, short throat at the tail of the stator hub followed by a conical diffuser.

An interesting and significant windfall of the optimized geometry is the unexpected effect that housing shape has on the flow straightening effectiveness of the diffuser. In the initial design, a residual amount of rotational velocity remains in the flow after passage through the stator. However, the optimized geometry has essentially zero rotational flow aft of its housing

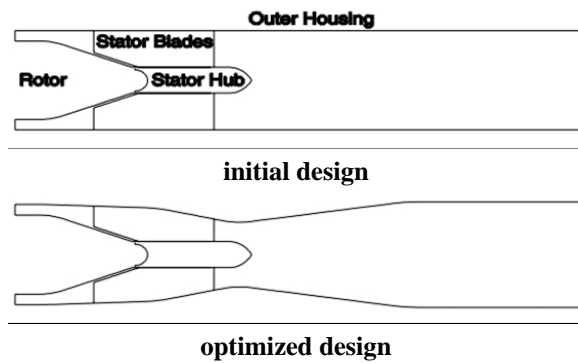


Figure 16. Cross-sectional view of outlet stator

throat, meaning that *all* of the rotational kinetic energy of the flow is being converted, in different degrees, to recovered pressure and hydraulic losses.

A second unexpected behavior of the optimized geometry is the complete absence of an unsteady 3D vortical structure in the blading section. This directly translates into a higher hydraulic efficiency since a source of wasteful energy dissipation has been eliminated by the shape optimization.

CONCLUSIONS

A systematic method of performing CFD-based design optimization has been developed and demonstrated as an effective tool for investigating means of cavitation delay. Localized regions of a geometry are parameterized using Non-uniform Rational B-Splines (NURBS), thus allowing local modifications to be controlled via a minimal number of design variables. An objective function is developed to maximize the local and average minimum pressure, where cavitation is observed to occur. Sensitivity derivatives are used to evaluate the dependence of the design variables to desired performance. An unstructured, finite-volume based RANS solver is used to analyze the modified designs. Hence, using a gradient-based approach, one can achieve optimal local modifications to suppress cavitation inception. This process was demonstrated for three example cases: an open-water propeller, a ducted propulsor, and the diffuser of a rotary blood pump. By locally distorting the propeller tip geometry, the average tip pressure can be raised by 22%. Moreover, in the case of ducted propulsion, it is shown that locally modifying the duct can completely de-couple the tip-leakage vortex interaction causing inception while simultaneously increasing the pressure in the trailing vortex. Finally, shape modifications in a rotary blood pump were shown to significantly increase surface washing while reducing rotational flow and suppressing vortex formation and shedding in the diffuser.

This systematic method has the potential to make significant changes in cavitation inception performance with negligible changes to thrust and torque. In the future, it is planned that a bubble dynamics solver be incorporated in the evaluation process, to be used as a more accurate objective function criteria for cavitation inception performance.

ACKNOWLEDGMENT

Support for this research was provided by Dr. Patrick Purtell of ONR under grant number N-00014-01-1-0455-01050428 and was monitored by Dr. Kihan Kim. This support is gratefully acknowledged. *Soli Deo gloria.*

REFERENCES

- [Anderson, 1998] Anderson, P., 1998. A comparative study of conventional and tip-fin propeller performance. In *Proceedings of the Twenty-Second Symposium on Naval Hydrodynamics*, pages 930–945. Washington, D.C.
- [Black, 1995] Black, S., 1995. The use of numerical optimization in advanced blade section design. In *Proceedings of 24th ATTC*. College Station, TX.
- [Brewer, 2002] Brewer, W. H., 2002. *On simulating tip-leakage vortex flow to study the nature of cavitation inception*. PhD thesis, Mississippi State University.
- [Brewer and Kinnas, 1997] Brewer, W. H. and Kinnas, S. A., 1997. Experiment and viscous flow analysis on a partially cavitating hydrofoil. *Journal of Ship Research*, 41(3):161–171.
- [Brewer et al., 2003] Brewer, W. H., Marcum, D., Jessup, S., Chesnakas, C., Hyams, D., and Sreenivas, K., 2003. An unstructured rans study of tip-leakage vortex cavitation inception. In *Proceedings of the International Symposium on Cavitation Inception, held at the 2003 ASME FED Summer Meeting in Honolulu, HI*, Honolulu, HI.
- [Burg and Newman, 2003] Burg, C. and Newman, J., 2003. Computationally efficient, numerically exact design space derivatives via the complex Taylor's series expansion method. *Computers and Fluids*, 32:373–383.
- [Burgreen and Antaki, 1996] Burgreen, G. W. and Antaki, J. F., 1996. CFD-based design optimization of a three-dimensional rotary blood pump. In *6th AIAA/USAF/NASA/ISSMO Symposium on Multidisciplinary Analysis and Optimization*, Bellevue, WA. AIAA 96-4185.
- [Burgreen and Antaki, 1998] Burgreen, G. W. and Antaki, J. F., 1998. CFD-based design optimization of the outlet stator of a rotodynamic cardiac assist device. In *7th AIAA/USAF/NASA/ISSMO*

- Symposium on Multidisciplinary Analysis and Optimization*, St. Louis, MO. AIAA 98-4808.
- [Burgreen et al., 2001] Burgreen, G. W., Antaki, J. F., Wu, Z., and Holmes, A. J., 2001. Computational fluid dynamics as a development tool for rotary blood pumps. *Artificial Organs*, 25(5):336–340.
- [Burgreen and Baysal, 1996] Burgreen, G. W. and Baysal, O., 1996. Three-dimensional aerodynamic shape optimization using discrete sensitivity analysis. *AIAA Journal*, 23(9):1761–1770.
- [Chesnakas and Jessup, 2003] Chesnakas, C. and Jessup, S., 2003. Tip-vortex induced cavitation on a ducted propulsor. In *Proceedings of the International Symposium on Cavitation Inception, held at the 2003 ASME FED Summer Meeting in Honolulu, HI*, Honolulu, HI.
- [Chorin, 1967] Chorin, A. J., 1967. A numerical method for solving incompressible viscous flow problems. *Journal of Computational Physics*, 2.
- [Coney, 1989] Coney, W. B., 1989. *A Method for the Design of a Class of Optimum Marine Propulsors*. PhD thesis, Massachusetts Institute of Technology. Department of Ocean Engineering.
- [Cowles and Martinelli, 2000] Cowles, G. and Martinelli, L., 2000. A control-theory based method for shape design in incompressible flow using rans. In *Proceedings of the Fluids 2000 Conference and Exhibit*, Denver, CO.
- [Crump, 1948] Crump, S. F., 1948. The effect of bulbous blade tips on the development of tip-vortex cavitation on model marine propellers. Technical report, David Taylor Model Basin.
- [Dreyer and Martinelli, 2000] Dreyer, J. and Martinelli, L., 2000. Hydrodynamic shape optimization of propulsor configurations using a continuous adjoining approach. In *Proceedings of the 15th AIAA Computational Fluid Dynamics Conference*, Anaheim, CA.
- [Farrell, 2000] Farrell, K., 2000. *An Eulerian/Lagrangian Computational Analysis for the Prediction of Cavitation Inception*. PhD thesis, Pennsylvania State University.
- [Farrell, 1987] Farrell, K. J., 1987. Tip clearance flow in axial-flow turbomachines: A review of the tip-wall vortex and subsequent cavitation in pumps. Technical Report N00024-85-C-6041, Applied Research Laboratory at the Pennsylvania State University.
- [Green and Duan, 1995] Green, S. I. and Duan, S. Z., 1995. The Ducted Tip – a hydrofoil tip geometry with superior cavitation performance. *Journal of Fluids Engineering*, 117:665–672.
- [Hino, 1999] Hino, T., 1999. Shape optimization of practical ship hull forms using navier-stokes analysis. In *7th International Conference on Numerical Ship Hydrodynamics*, Nantes, France.
- [Hirsch, 1994a] Hirsch, C., 1994a. *Numerical Computation of Internal and External FLOws, Volume 1*. John Wiley & Sons.
- [Hirsch, 1994b] Hirsch, C., 1994b. *Numerical Computation of Internal and External FLOws, Volume 2: Computational Methods for Inviscid and Viscous FLOws*. John Wiley & Sons.
- [Hyams, 2000] Hyams, D., 2000. *An Investigation of Parallel Implicit Solution Algorithms for Incompressible FLOws on Unstructured Topologies*. PhD thesis, Mississippi State University.
- [Jameson, 1988] Jameson, A., 1988. Aerodynamic design via control theory. *Journal of Scientific Computing*, 3(2):233–260.
- [Jessup, 2000] Jessup, S. D., 2000. Private conversations. Naval Surface Warfare Center, Carderock Division, West Bethesda, MD.
- [Jia et al., 2001] Jia, X., Wang, Z., and Cai, R., 2001. Numerical investigation of different tip gap shape effects on aerodynamic performance of an axial-flow compressor stator. In *Proceedings of ASME TURBO EXPO*.
- [Judge et al., 2001] Judge, C., Oweis, G., Ceccio, S., Jessup, S., Chesnakas, C., and Fry, D., 2001. Tip-leakage vortex inception on a ducted rotor. In *Proceedings of the CAV2001 Fourth International Symposium on Cavitation*. Pasadena, CA.
- [Kerwin, 1973] Kerwin, J., 1973. Computer techniques for propeller blade design. *International Shipbuilding Progress*, 20(227).
- [Kerwin et al., 1994] Kerwin, J., Keenan, D., Black, S., and Diggs, J., 1994. A coupled viscous/potential flow design method for wake adapted multi-stage, ducted propulsors using generalized geometry. *Trans. SNAME*, 102.
- [Kuiper, 2001] Kuiper, G., 2001. New developments around sheet and tip vortex cavitation on ships' propellers. In *Proceedings of the CAV2001 Fourth International Symposium on Cavitation*.
- [Marcum and Weatherill, 1995] Marcum, D. L. and Weatherill, N. P., 1995. Unstructured grid generation using iterative point insertion and local reconnection. *AIAA*, 33(9):1619–1625.
- [Mishima, 1996] Mishima, S., 1996. *Design of Cavitating Propeller Blades in Non-Uniform FLOW by Numerical Optimization*. PhD thesis, Massachusetts Institute of Technology.
- [Newman et al., 1998] Newman, J. C., Anderson, W., and Whitfield, D., 1998. Multidisciplinary sensitivity derivatives using complex variables. Technical report, Mississippi State University.
- [Newman et al., 1999] Newman, J. C., Taylor, A. C., Barnwell, R. W., Newman, P. A., and Hou, G. J.-W., 1999. Overview of sensitivity analysis and shape optimization for complex aerodynamic con-

- figurations. *Journal of Aircraft*, 36:87–96.
- [Platzer and Souders, 1979] Platzer, G. P. and Souders, W. G., 1979. Tip vortex cavitation delay with application to marine lifting surfaces. Technical report, David W. Taylor Naval Ship Research and Development Center.
- [Ragab, 2001] Ragab, S., 2001. Shape optimization in free surface potential flow using an adjoint formulation: surface ships. In *Proceedings of the 31st AIAA Fluid Dynamics Conference*, Anaheim, CA.
- [Shuba, 1983] Shuba, B. H., 1983. An investigation of tip-wall vortex cavitation in an axial-flow pump. Master's thesis, The Pennsylvania State University, Department of Aerospace Engineering.
- [Soto and Löhner, 2001] Soto, O. and Löhner, R., 2001. CFD shape optimization using an incomplete-gradient adjoint formulation. *International Journal of Numerical Methods in Engineering*, 51(1):735–753.
- [Souders and Platzer, 1981] Souders, W. G. and Platzer, G. P., 1981. Tip vortex cavitation characteristics and delay of inception on a three-dimensional hydrofoil. Technical Report DTNSRDC-81/007, David W. Taylor Naval Ship Research and Development Center.
- [Spalart and Allmaras, 1992] Spalart, P. R. and Allmaras, S. R., 1992. A one-equation turbulence model for aerodynamic flows. *AIAA*.
- [Tahara et al., 2000] Tahara, Y., Paterson, E., Stern, F., and Himeno, Y., 2000. CFD-based optimization of naval/surface combatant. In *Proceedings of the 23rd Symposium on Naval Hydrodynamics*, Val de Reuil, France.